HHS Public Access

Author manuscript

Am J Ophthalmol. Author manuscript; available in PMC 2020 December 01.

Published in final edited form as:

Am J Ophthalmol. 2019 December ; 208: 111–123. doi:10.1016/j.ajo.2019.07.003.

Quantification of choriocapillaris with OCTA: a comparison study

Zhongdi Chu[1], **Giovanni Gregori**[2], **Philip J Rosenfeld**[2], **Ruikang K Wang**[1,3]

[1.]Department of Bioengineering, University of Washington, Seattle, Washington

[2.]Department of Ophthalmology, Bascom Palmer Eye Institute, University of Miami Miller School of Medicine, Miami, Florida, United States

[3.]Department of Ophthalmology, University of Washington, Seattle, Washington

Abstract

Purpose—To demonstrate the variation in quantitative choriocapillaris (CC) metrics with various binarization approaches using optical coherence tomography angiography (OCTA).

Design—Retrospective, observational, cross-sectional case series.

Methods—3×3 mm and 6×6 mm macular OCTA scans were obtained from normal eyes and from eyes with drusen secondary to AMD. The CC slab was extracted and the CC flow deficits (FDs) were segmented with two previously published algorithms: fuzzy C-means approach (FCM method) and Phansalkar's local thresholding (Phansalkar method). Four different values for the radius were used in order to investigate the effect on the FD segmentation when using the Phansalkar method. FD density (FDD), mean FD size (MFDS), FD number (FDN), FD area (FDA) and inter-capillary distance (ICD) were calculated for comparison. Repeatability was assessed as coefficient of variation (CV) and Pearson's correlation analysis was conducted.

Results—Six eyes from 6 subjects with normal eyes and 6 eyes from 6 subjects with drusen secondary to AMD were scanned. 3×3 mm scans resulted in higher repeatability compared to 6×6 mm scans. For the Phansalkar method, larger values of the radius resulted in higher repeatability. ANOVA tests resulted in significant differences ($p<0.001$) among the FCM method and the Phansalkar method with different radius options, for all CC metrics and scan sizes investigated. In 3×3 mm scans, significant correlation was found between the FCM method and the Phansalkar method for all quantitative CC metrics other than FDN (all $p<0.001$, $0.90<r<0.99$).

Conclusions—Quantitative CC analysis with commercially available OCTA is complicated and researchers need to pay close attention on how they conduct such analysis.

Corresponding Author: Ruikang K Wang, University of Washington, Box 355061, 3720 15th Ave NE, Seattle, WA 98195-5061, Phone: 206 616 5025, Fax: 206 685 3300, wangrk@uw.edu.

INTRODUCTION

Choriocapillaris (CC) is a thin but dense vascular monolayer located beneath Bruch's membrane (BM) in the inner choroid. Multiple histopathological reports have shown that there are correlations between CC integrity and ocular diseases such as age-related macular degeneration (AMD), diabetic retinopathy, and uveitis[1–4]. While the ability to perform *in vivo* quantitative imaging of the CC would be of great clinical value, only recently has the advent optical coherence tomography (OCT) based angiography (OCTA) made this possible, with depth resolved capability and high spatial resolution (~15–20 μm laterally, ~6 μm axially) suitable for vasculature quantification.[5, 6] Many researchers have reported useful quantitative parameters, for example, vessel area density (VAD), vessel skeleton/length density (VSD/VLD), vessel diameter index (VDI), vessel complexity index and flow impairment zone; all of which may be used to describe retinal vasculature abnormalities in various ocular diseases[7–14]. Such ability to quantify the vasculature is attributed to the power of OCTA to resolve the microvascular networks of the retina because the inter-capillary distances (ICDs) are generally larger (71.30 ± 5.17 μm [15]) than the system's lateral resolution (~15–20 μm). However, we should be aware that if two vessels are separated with a distance similar to or less than the system's lateral resolution, then OCTA would not be able to tell them apart. Unlike the retinal microvasculature, the CC is a much denser capillary network. Histological studies[16–19] have revealed that the CC vasculature has different morphological appearances in different regions: a dense honeycomb network of freely interconnected capillaries separated by septa in the submacular region and a polygonal lobular network in the equatorial and peripheral regions. The ICD ranges from 5–20 μm in the posterior pole to 20–300 μm in equatorial and peripheral regions. [18] Given the wide range of the CC ICDs, the current commercial OCTA systems would not always be able to resolve the CC vasculature, particularly in the posterior pole region where the CC abnormalities are thought to be closely related to the development of AMD. Consequently, it remains problematic to directly visualize the CC vasculature from OCTA images.

Rather than visualize the CC vasculature directly, many researchers have chosen to segment and quantify CC flow deficits (FDs)[20–29], which should indicate an impairment of CC flow or flow that is below the OCTA detection sensitivity. By definition, the flow deficit must have a size that is larger than the normal ICD, which may be within the capability of OCT system to resolve. Several different algorithms for CC FD segmentation have been reported. Al-Sheikh et al. (2017) reported a method of segmenting the CC FDs using Otsu's global thresholding[25]. However, the assumption of Otsu's method is that the image histogram should follow a bimodal distribution[30], which unfortunately is not the case for OCTA CC images. Alten et al. (2016), Nesper et al. (2017) and Borrelli et al. (2018) reported a method of segmenting the CC FDs using the mean pixel value in the outer retinal layer (ORL) as a global threshold[31–33]. This approach relies on the assumption that the ORL and CC layer share the same systemic noise characteristics, but this is not the case because the CC lies under the retinal pigment epithelium (RPE) complex, which raises the noise floor due to its high scattering nature. Carnevali et al. (2017) reported CC FD segmentation using the mean pixel value in the CC layer as a global threshold[34]. This approach is problematic because the CC vasculature is extremely dense, and it is almost impossible to use the mean pixel value as

the cutoff threshold between flow and absence of flow. Moreover, Sugano et al. (2018) used a method commonly seen in retinal vasculature analyses: hessian filter to segment CC vasculature [35] This approach is also invalid because OCTA cannot resolve the CC vasculature in the posterior pole and there are no tube-like structures for hessian filter to work with.

As a method designed for binarization of low contrast images[36], Phansalkar's local thresholding method in Image J (National Institutes of Health, Bethesda, Maryland, USA) has become one of the most popular methods for the CC FD segmentation[21, 25, 26, 37–42] Most researchers have chosen a 15-pixel radius in the analysis, regardless of the actual properties (i.e. actual pixel size) of different OCTA CC images. For example, Spaide et al. first reported in 2016 the use of a 15-pixel radius (~148 μm) with 304×304 pixel 3×3 mm OCTA images[26] but later in 2018 reported the use of the same 15-pixel radius (~88 μm) with 512×512 pixel 3×3 mm OCTA images[43]. Other researchers have reported using the same 15-pixel radius with 1024×1024 pixel 3×3 mm OCTA images[40] (~44 μm) as well as 1024×1024 pixel 6×6 mm OCTA images[39, 40](~88 μm). The lack of consistency in the physical dimensions of the radius could affect the application of the Phansalkar method and lead to discrepancies in CC FD measurements. Recently, a more reliable method, based on a fuzzy C-means self-clustering algorithm, has been reported to segment the CC FDs[22]. This method automatically assigns all pixels in an OCTA CC image into different clusters based on histogram distribution. It also utilizes localized information to remove noise after clustering. The cluster with the lowest intensity is then identified as the FDs while other clusters are identified by the region occupied by the CC vasculature. This approach was used to measure the average ICD in the macular CC of subjects with normal eyes, which was found to be around 24 μm using power spectrum analysis[22].

Given the increasing interests in quantitative studies of the CC, there is a pressing need to investigate and understand how CC quantification can be conducted in a thoughtful and reproducible way. Several factors could potentially greatly affect CC quantification, such as scan signal intensity, correct CC slab segmentation, effective CC FD segmentation and appropriate selection of CC quantitative parameters. In this study, we compare the results of different CC FD segmentation algorithms on 3×3 mm and 6×6 mm OCTA scans of both normal eyes and eyes with drusen as the basis to discuss the necessary steps and precautions for proper CC quantification.

METHODS

This retrospective, cross-sectional study was performed at the University of Miami and the University of Washington. The Institutional Review Board of the University of Miami Miller School of Medicine and the Institutional Review Board of Medical Sciences Subcommittee at the University of Washington, Seattle, approved this study. The tenets of the Declaration of Helsinki and the Health Insurance Portability and Accountability Act of 1996 regulations were followed. Written informed consents were obtained from all subjects before participation. Six subjects with a normal ocular history, no visual complains, and no identified optic disc, retinal, or choroidal pathologies on examination and six subjects with

drusen secondary to intermediate AMD were enrolled in the study from January 2017 to March 2017.

Imaging acquisition

All subjects were scanned in both eyes using the PLEX® Elite 9000 (Carl Zeiss Meditec, Dublin, CA), a swept-source OCTA (SS-OCTA) instrument that employed a 100 kHz light source with a 1060 nm central wavelength and a 100 nm bandwidth, providing an axial resolution of ~ 5.5μm and a lateral resolution of ~20 μm estimated at the retinal surface[44]. For each eye, both 3×3 mm and 6×6 mm scans centered at the fovea were repeated three times, yielding 6 scans in total. The right eyes were selected for the analysis unless low signal strength (<7) or severe motion artifacts were present. For the 3×3 mm scans, 300 A-lines were acquired for each B-scan and 300 sets of 4 repeated B-scans were acquired for each C-scan, yielding a digital resolution of 10 μm/pixel. For the 6×6 mm scans, 500 A-lines were acquired for each B-scan and 500 sets of 2 repeated B-scans were acquired for each C-scan, yielding a digital resolution of 12 μm/pixel.

Image processing

After acquiring volumetric OCTA data, two approaches were used to identify the CC slab for later FD segmentation: a semi-automated segmentation software[45] and the automated segmentation provided by the PLEX® Elite. We employed the semi-automated segmentation software[45] to obtain an accurate segmentation of RPE/BM complex and to extract the CC slabs. In addition, we also produced *en face* CC OCTA images using automated segmentation software on the PLEX® Elite. Automated segmentation does a fair job in segmenting the RPE/BM boundary in normal eyes. However, in diseased eyes, this is more problematic. For example, in eyes with drusen, the RPE is deformed and the RPE-fit segmentation from the automated algorithm on the instrument gives a better approximation of the BM location. Therefore, we used the RPE-fit as the reference boundary to extract the CC slab in these eyes, whereas the RPE boundary was used for the normal eyes. However, segmentation errors could still be present even with our RPE-fit scheme, therefore we have chosen to conduct all our quantitative analysis on images produced by semi-automated segmentation.

The CC slab was defined as a 15 μm thick slab, starting 16 μm under the RPE (or BM, in cases of RPE/BM separation)[23], for both segmentation approaches. *En face* images were produced using a maximum projection and possible signal attenuation caused by the RPE/BM complex was compensated for using a previous reported strategy[20]. Retinal projection artifacts were subsequently removed[46] and the corresponding regions were excluded in further analyses. 3×3 mm images were resized as 600×600 pixels (2x magnification from raw OCTA data) and 6×6 mm images were resized as 1000×1000 pixels (2x magnification from raw OCTA data), yielding a pixel size of 5 μm in 3×3 scans and 6 μm in 6×6 scans. To reduce the variability of the signal strength among the subjects, all the OCT volumetric data were normalized to a signal strength of nine before the OCTA maps were processed[47].

CC slabs generated by the semi-automated segmentation approach were selected for further quantification (Figure 1: A, D, G). Two methods were used for CC FD segmentation: our previously published complex thresholding strategy[22] using a fuzzy C-means algorithm (the FCM method) and the Phansalkar's local thresholding method (the Phansalkar method) provided in Image J. Previous studies utilizing the Phansalkar method had all chosen a 15-pixel radius regardless of image size[21, 25, 26, 37–42] However, the proper use of this method has to consider the physical dimensions of the image, which involves the size of pixels, rather than the pixel numbers in its radius kernel for segmenting the FDs. In this study, to investigate how the radius size would have an effect on the FD segmentation and quantification, we used four different radius options: in 3×3 mm scans, 2 pixels (10 μm, the digital resolution of 3×3 mm scans), 5 pixels (25 μm, around the normal ICD in macular CC), 12 pixels (60 μm), 15 pixels (75 μm) and 30 pixels (150 μm); in 6×6 mm scans, 2 pixels (12 μm, the digital resolution of 6×6 mm scans), 4 pixels (24 μm, around the normal ICD in macular CC), 10 pixels (60 μm), 15 pixels (90 μm) and 25 pixels (150 μm). After CC FD segmentation (Figure 1: B, E H, the FCM method), FDs with an equivalent diameter smaller than 24 μm were excluded from further analysis[22] (Figure 1: C, F, I, using the FCM method).

After CC FD segmentation and binarization, quantitative metrics to describe FDs were calculated, including FD density (FDD), FD number (FDN), mean FD size (MFDS), ICD and total FD area (FDA). FDD was defined as the percentage of image area of no flow to the total image area. FDD and CC vessel density add up to 1. FDN was defined as the total number of FDs detected and MFDS was defined as the average area of individual FDs ICD was calculated as the average minor axis of the ellipses that have the same normalized second central moments of the detected FDs. FDA was calculated as the total area occupied by FDs. Lengths were always measured in μm and areas in μm^2.

Statistical analysis

Statistical analyses were performed using MATLAB (R2016b; MathWorks, Inc, Natick, Massachusetts, USA). Descriptive statistics were reported as mean and standard deviation (SD). Repeatability was calculated using 3 repeated scans of each subject on the same visit, in the form of intra-class correlation (ICC) with the two-way mixed, single measures, absolute agreement model[48]. ANOVA test was used to compare quantitative CC metrics among different methods. Correlation among different methods were analyzed using Pearson's correlation, both r values and p values were reported. P values smaller than 0.05 were considered statistically significant.

RESULTS

The CC is a thin slab beneath the BM and OCTA CC slab appearance can vary significantly if the slab is too close to the RPE or too close to Sattler's layer. Figure 2 demonstrates the appearances of CC OCTA slabs (Figure 2: A–E), OCT structural slabs (Figure 2: F–J) and OCT B-scans with segmentation lines (Figure 2: K–O) when the start position for CC slab was selected differently relative to the RPE position. Machine output CC slabs from PLEX® Elite are defined as +29 μm to +49 μm under the RPE segmentation line (Figure 2.E, J,O),

where it appears that the slab may be too deep into the Sattler's layer due to heterogeneous appearances caused by melanocytes.

Repeatability Study

Six subjects with normal eyes and six subjects with drusen secondary to AMD were recruited for the repeatability study. For each subject, both 3×3 mm and 6×6 mm scans were acquired three times at the same visit. Figure 1, panels A, D, and G show an example of the three repeated 3×3 mm scans while panels J, M and P show an example of the three repeated 6×6 mm scans. Both the FCM method and the Phansalkar method with four different radius choices were used to perform quantitative analyses of CC on each of the 3×3 mm and 6×6 mm averaged scans. Figure 3 demonstrates an example of CC FD segmentation using both the FCM method (Figure 3: B, I) and the Phansalkar method (Figure 3: C–G and J–N) in both scan sizes for the normal eye. Figure 4 shows the same analysis for a subject with drusen. Qualitatively speaking, the Phansalkar method with larger radius options resulted in more FDs segmented in the same CC image.

Repeatability was assessed using the ICC with the two-way mixed, single measures, absolute agreement model. Table 1 shows the ICC values for both the FCM method and the Phansalkar method for various radius options in 3×3 mm scans of normal eyes and Table 2 shows the ICC values in 3×3 mm scans of eyes with drusen. When using the Phansalkar method, larger radius options tended to result in higher repeatability, likely because higher radius option leads to more and larger FD segmentations. Similarly, Table 3 and 4 demonstrates the repeatability of both methods in normal and drusen for 6×6 mm scans, respectively. For both methods, the 3×3 mm scans resulted in higher repeatability compared to the 6×6m mm scans.

Correlation analysis

All twelve subjects were grouped and analyzed for correlations between the FCM method and the Phansalkar method. Only one scan was selected from three repeated scans with the highest signal strength, resulting in twelve 3×3 mm scans and twelve 6×6 mm scans. Table 5 shows the mean and standard deviation (SD) values of various quantitative CC metrics in 3×3 mm scans and Table 6 shows the same for 6×6 mm scans. In both 3×3 mm and 6×6 mm scans, the Phansalkar method with larger radius options typically resulted in larger FDD, MFDS, ICD and FDA values. ANOVA tests showed that quantitative CC metrics generated by the different methods are not equivalent.

Pearson's correlation was assessed between quantitative CC metrics using the FCM method and the Phansalkar method, and Table 7 reports the corresponding r and p values for the 3×3 mm scans and Table 8 for the 6×6 mm scans. In the 3×3 mm scans, except for FDN, the Phansalkar method showed significant correlation with the FCM method, regardless of radius options. Such correlations were strongest with a 2-pixel radius option, and decreased for larger radii. In the 6×6 mm scans, the r values are smaller compared to those in the 3×3 mm scans, indicating weaker correlations. The 4-pixel radius (24 μm) option was the only radius option that resulted in significant correlation with the FCM method for all quantitative CC metrics.

DISCUSSION

Visualizing and quantifying the CC in vivo has been a keen interest of many investigators over the decades, especially since the recent technological advances in commercial OCTA systems. However, researchers should stay cautious and vigilant when conducting quantitative analyses of the CC using OCTA images. There are several important factors that we should be aware that could potentially affect the results of CC quantification.

The first one is the signal intensity. All reported CC FD segmentation methods have used some form of intensity thresholds since morphological filters do not apply. The caveat of using intensity thresholds is that it requires high quality OCTA scans. If the scan signal strength is too low, or partially out of focus, CC OCTA images will appear darker than normal, and this could lead to false positive identifications of CC FDs. More dangerously, when anatomical abnormalities above CC are present, it could block OCT signals. The consequence is the creation of shadows in OCTA CC images, giving rise to false positive CC FDs identification. In order to counteract such situations, an OCT signal compensation strategy[20] should be considered for the attenuated signals detected from structural OCT images. In this study, we only included scans with a signal strength index higher than 7, according to manufacturer's recommendation. Future studies are warranted to investigate if signal strength plays a role in CC quantification.

Another important consideration is the location of the CC slab segmentation. Because the CC is such a thin layer (10μm~20μm[23, 49], which represents as 5~10 pixels in PLEX® Elite), the analysis can be quite sensitive to the distance between the thickness of the CC slab and its distance from the RPE. Figure 2 demonstrates that in commercial systems, the default CC slab might not be optimal, and researchers need to be cautious in using the default slab. This could become even more problematic in pathological cases, because the automatic identification of RPE (or BM) is often incorrect. On PLEX® Elite instruments, researchers might be better off using a CC slab defined by RPE-fit segmentation rather than the default RPE segmentation since accurate CC quantification is almost impossible without accurate CC slab segmentations. Therefore, before a robust automatic segmentation software is rigorously validated, semi-automated segmentation software[45] should be considered because it would ensure the correct identification of the CC slab to the best of our abilities.

Caution is also needed for the segmentation of FDs. Most methods of CC FD segmentation reported so far have used intensity threshold approaches. Using a single global intensity threshold across all cases can be problematic because of signal variability both within scans and across different scans and subjects. As we have mentioned in the introduction, many of these global intensity thresholding approaches are not appropriate for CC FDs segmentation. Many researchers have also used Phansalkar's local thresholding method with a fixed 15-pixel radius, regardless of the pixel sizes. However, a proper selection of the local window radius should be based on actual size (in microns) rather than the number of pixels. Too large a window can artificially overestimate the extent of FDs. The present study found that different radius options (10 μm to 150 μm) can lead to different quantitative CC metrics and different repeatability. In this study, we chose to resize the images by a factor of 2. 3×3 mm images originally have 300×300 pixels and we resized it to 600×600 pixels. 6×6 mm images

originally have 500×500 pixels and we resized it to 1000×1000 pixels. Moreover, the Phansalkar method in 3×3 mm scans of eyes with drusen seems to over identify CC FD areas. This is possibly because the Phansalkar method is designed for low contrast image segmentation. The threshold used in Phansalkar's method is positively correlated with the standard deviation value of the image, which is also positively correlated with image contrast. In cases of extensive CC loss, the OCTA CC image becomes higher contrast, this could lead to a higher threshold value and more CC FDs areas identified. Such situation could potentially violate the low contrast image assumption for the Phansalkar's method but further investigations are warranted for a conclusive statement. Our analysis have also shown that the FCM method and Phansalkar's method all provided satisfactory repeatability. ICC values are the highest in 3×3 mm normal scans and lowest in 6×6 drusen scans. To further reduce variation, researchers should consider average multiple CC scans.[22] Larger radius options in the Phansalkar's method also tend to result in higher ICC values. Our group has also reported a novel CC FD segmentation method using the mean and SD value from normal population[20]. This SD method has showed significant correlation with the FCM method using a normative database[50].

Another concern is the choice of OCTA scan size. All scan sizes from the same OCTA system share the same lateral resolution, but the digital resolutions (determined by the sampling density) may vary. High speed SS-OCTA system[49] can provide denser scans (~4 μm/pixel) with more repeated B-scans (~10 repeats) and provide higher CC imaging quality. In the PLEX® Elite, the 3×3 mm scan uses 4 repeated B-scans for OCTA and has a digital resolution of 10 μm/pixel. The 6×6 mm scan uses 2 repeated B-scans for OCTA and has a digital resolution of 12 μm/pixel. The 6×6 mm scan contains a larger area at the cost of digital resolution and signal to noise ratio (SNR). Both scan sizes have been reported to be useful in quantitative CC analyses. As indicated by our results (Figure 3 and Figure 4), the appearances of CC FDs are similar in 3×3 mm and 6×6 mm images but do not present the exactly same image contrast. The PLEX® Elite also provides 9×9 mm, 12×12 mm and 9×15 mm scans, all using 2 repeated B-scans for OCTA and providing a digital resolution of 18 μm/pixel, 24 μm/pixel and 18 μm/pixel, respectively. Larger scans are valuable because not all pathologies are contained within the 6×6 mm macular region, but they also offer lower digital resolution, lower SNR, and a longer scan time that increases the probability of having motion artifacts. Researchers need to pay extreme caution when using larger sized scans for CC quantification. Moreover, the thickness of the CC layer varies from macula region to equatorial regions, and a uniformly defined thickness of the CC slab will certainly introduce errors.

Lastly, given currently available clinical systems, researchers need to pay attention to what quantifiable parameters can be meaningfully calculated from the CC images. In retinal analysis, parameters such as vascular area density (VAD), vessel skeleton density (VSD), vessel length density (VLD) and vasculature diameter index (VDI), have been used[7]. These quantitative parameters are valid because the retinal inter-capillary distance is much larger than the system lateral resolution and OCTA can resolve the retinal vasculature. Therefore, morphological filters may be used to binarize retinal vessels. However, parameters like VSD/VLD and VDI are not applicable to the CC vasculature given the lateral resolution of current OCTA systems. As we have explained before, ICDs in the CC are too small and

OCTA simply cannot resolve the CC vasculature. Because of this technical limitation, we are only able to examine non-perfusion in CC (FDs) but not detailed morphological vascular patterns. Moreover, when CC FD segmentation is performed with the Phansalkar method, the VDI is highly dependent on the size of radius, and a larger radius option would generally lead to wider segmentation of CC vasculature and larger VDI. Therefore, measurements of VSD/VLD and VDI for the CC vasculature are substantially meaningless, at least in the macula, using the current OCTA resolution.

We have only examined CC quantification with SS-OCTA in this study, not spectral domain OCTA (SD-OCTA). SS-OCTA is superior to SD-OCTA in choroidal imaging due to the deeper penetration with a longer wavelength and less sensitivity rolloff[51]. SD-OCTA may still be useful in quantitative CC analysis. However, greater caution needs to be paid to scan quality in SD-OCTA images. Low quality scans can lead to false positive identification of FDs. SS-OCTA and SD-OCTA systems generally have different SNR and researchers might need to optimize their CC algorithms accordingly from one system to another. Future studies are warranted to investigate how SS-OCTA and SD-OCTA compare in quantitative CC analyses.

In this study, we compared two different CC FD segmentation methods: the FCM method and the Phansalkar method with different radius options. We utilized repeated scans from six subjects with normal eyes and six AMD drusen subjects to assess repeatability of each method. Overall, our results indicate that 3×3 mm scans yield better repeatability than 6×6 mm scans. When using the Phansalkar method, larger radius options resulted in larger FD areas being segmented and typically lower CV. Our data strongly suggests that the radius choice in the Phansalkar method is very important and researchers using this approach for CC analysis should be extremely careful in the proper use of radius parameter. When comparing quantitative CC metrics produced by both methods, 3×3 mm scans also showed stronger correlation among methods than 6×6 mm scans.

We have chosen to use six quantitative CC metrics of FDD, FDA, FDN, MFDS and ICD. To the best of our knowledge, this is the first time ICD has been reported using the approximation of minor axis, all other metrics have been reported by various groups previously. FDD, FDA, MFDS and FND could all be derived from each other. We chose to report all these four metrics because of their popularity in the literature, for future studies, researcher might not need to report them all. The correlation among those metrics could also lead to false significant p values when multiple comparisons are conducted. This is not the case for our study (TABLE 5 and TABLE 6) as our p values are all smaller than 0.001, still significant after Bonferroni correction.

There are some limitations in our study. Firstly, there is a lack of ground truth for CC vasculature. Traditional dye-based angiography cannot provide detailed CC imaging suitable for quantification. Adaptive optics OCTA and higher speed SS-OCTA lab-built systems have demonstrated high resolution images, yet smaller fields of view for CC imaging[23, 49]. We chose to use OCTA CC data acquired by a commercially available OCT system for clinical relevance. Secondly, we have a limited sample size. The purpose of this study was to

demonstrate differences in different CC algorithms, and how those methods really compare needs to be studied further with a larger dataset.

In summary, we have demonstrated that CC quantitative analysis with commercial OCTA systems can be complicated. Researchers need to pay close attention to how they choose to conduct such analysis in the future.

ACKNOWLEDGMENTS/DISCLOSURES

a. Funding/Support: Research supported by grants from the National Eye Institute (R01EY024158, R01EY028753), the Salah Foundation, Carl Zeiss Meditec, an unrestricted grant from the Research to Prevent Blindness, Inc., New York, NY, and the National Eye Institute Center Core Grant (P30EY014801) to the Department of Ophthalmology, University of Miami Miller School of Medicine. The funding organization had no role in the design or conduct of this research.

b. Financial Disclosures: Dr. Gregori, Dr. Wang and Dr. Rosenfeld received research support from Carl Zeiss Meditec, Inc. Dr. Gregori and the University of Miami co-own a patent that is licensed to Carl Zeiss Meditec, Inc.

Dr. Rosenfeld is a consultant for Apellis, Boehringer-Ingelheim, Carl Zeiss Meditec, Chengdu Kanghong Biotech, Ocunexus Therapeutics, Genentech, Healios K.K, Hemera Biosciences, F. Hoffmann-La Roche Ltd., Isarna Pharmaceuticals, Ocunexus, Ocudyne, and Unity Biotechnology. He also has equity interest in Apellis, Verana Health, and Ocudyne.

Dr. Wang discloses intellectual property owned by the Oregon Health and Science University and the University of Washington. Dr. Wang also receives research support from Tasso Inc, Moptim Inc, Colgate Palmolive Company and Facebook technologies LLC. He is a consultant to Insight Photonic Solutions, Kowa, and Carl Zeiss Meditec.

The remaining authors have no disclosures.

c. Other Acknowledgments: None

REFERENCES

1. Cao J, McLeod DS, Merges CA, Lutty GA. Choriocapillaris degeneration and related pathologic changes in human diabetic eyes. Arch Ophthalmol 1998;116:(5):589–597. [PubMed: 9596494]
2. Lutty G, Grunwald J, Majji AB, Uyama M, Yoneya S. Changes in choriocapillaris and retinal pigment epithelium in age-related macular degeneration. Mol Vis 1999;5:(35):35. [PubMed: 10562659]
3. Bhutto I, Lutty G. Understanding age-related macular degeneration (AMD): relationships between the photoreceptor/retinal pigment epithelium/Bruch's membrane/choriocapillaris complex. Mol Aspects Med 2012;33:(4):295–317. [PubMed: 22542780]
4. Nazari H, Hariri A, Hu Z, Ouyang Y, Sadda S, Rao NA. Choroidal atrophy and loss of choriocapillaris in convalescent stage of Vogt-Koyanagi-Harada disease: in vivo documentation. J Ophthalmic Inflamm Infect 2014;4:(1):9. [PubMed: 24655594]
5. Chen C-L, Wang RK. Optical coherence tomography based angiography. Biomed Opt Express 2017;8:(2):1056–1082. [PubMed: 28271003]
6. Kashani AH, Chen C-L, Gahm JK, et al. Optical coherence tomography angiography: A comprehensive review of current methods and clinical applications. Prog Retin Eye Res 2017.
7. Chu Z, Lin J, Gao C, et al. Quantitative assessment of the retinal microvasculature using optical coherence tomography angiography. J Biomed Opt 2016;21:(6):066008–066008.
8. Kim AY, Chu Z, Shahidzadeh A, Wang RK, Puliafito CA, Kashani AH. Quantifying Microvascular Density and Morphology in Diabetic Retinopathy Using Spectral-Domain Optical Coherence Tomography AngiographyQuantifying Vascular Changes in DR With SD-OCTA. Invest Ophthalmol Vis Sci 2016;57:(9):OCT362–OCT370. [PubMed: 27409494]

9. Kim AY, Rodger DC, Shahidzadeh A, et al. Quantifying Retinal Microvascular Changes in Uveitis Using Spectral-Domain Optical Coherence Tomography Angiography. Am J Ophthalmol 2016;171:101–112. [PubMed: 27594138]
10. Koulisis N, Kim AY, Chu Z, et al. Quantitative microvascular analysis of retinal venous occlusions by spectral domain optical coherence tomography angiography. PLoS ONE 2017;12:(4):e0176404. [PubMed: 28437483]
11. Richter GM, Madi I, Chu Z, et al. Structural and Functional Associations of Macular Microcirculation in the Ganglion Cell-Inner Plexiform Layer in Glaucoma Using Optical Coherence Tomography Angiography. J Glaucoma 2018;27:(3):281–290. [PubMed: 29394201]
12. Chen C-L, Bojikian KD, Gupta D, et al. Optic nerve head perfusion in normal eyes and eyes with glaucoma using optical coherence tomography-based microangiography. Quant Imaging MedSurg 2016;6:(2):125.
13. Jia Y, Bailey ST, Hwang TS, et al. Quantitative optical coherence tomography angiography of vascular abnormalities in the living human eye. Proceedings of the National Academy of Sciences 2015;112:(18):E2395–E2402.
14. Samara WA, Shahlaee A, Sridhar J, Khan MA, Ho AC, Hsu J. Quantitative optical coherence tomography angiography features and visual function in eyes with branch retinal vein occlusion. Am J Ophthalmol 2016;166:76–83. [PubMed: 27038893]
15. Chan G, Balaratnasingam C, Xu J, et al. In vivo optical imaging of human retinal capillary networks using speckle variance optical coherence tomography with quantitative clinico-histological correlation. Microvasc Res 2015;100:32–39. [PubMed: 25917012]
16. Torczynski E, Tso MO. The architecture of the choriocapillaris at the posterior pole. Am J Ophthalmol 1976;81:(4):428–440. [PubMed: 1266921]
17. Yoneya S, Tso MO, Shimizu K. Patterns of the choriocapillaris. Int Ophthalmol 1983;6:(2):95–99. [PubMed: 6403481]
18. Olver J Functional anatomy of the choroidal circulation: methyl methacrylate casting of human choroid. Eye 1990;4:(2):262–272. [PubMed: 2379644]
19. Fryczkowski AW. Anatomical and functional choroidal lobuli. Int Ophthalmol 1994;18:(3):131–141. [PubMed: 7852018]
20. Zhang Q, Zheng F, Motulsky EH, et al. A Novel Strategy for Quantifying Choriocapillaris Flow Voids Using Swept-Source OCT Angiography. Invest Ophthalmol Vis Sci 2018;59:(1):203–211. [PubMed: 29340648]
21. Borrelli E, Souied EH, Freund KB, et al. REDUCED CHORIOCAPILLARIS FLOW IN EYES WITH TYPE 3 NEOVASCULARIZATION AND AGE-RELATED MACULAR DEGENERATION. Retina 2018;38(10):1968–1976. [PubMed: 29746411]
22. Chu Z, Zhou H, Cheng Y, Zhang Q, Wang RK. Improving visualization and quantitative assessment of choriocapillaris with swept source OCTA through registration and averaging applicable to clinical systems. Sci Rep 2018;8:(1):16826. [PubMed: 30429502]
23. Kurokawa K, Liu Z, Miller DT. Adaptive optics optical coherence tomography angiography for morphometric analysis of choriocapillaris. Biomedical Optics Express 2017;8:(3):1803–1822. [PubMed: 28663867]
24. Al-Sheikh M, Falavarjani KG, Pfau M, Uji A, Le PP, Sadda SR. Quantitative Features of the Choriocapillaris in Healthy Individuals Using Swept-Source Optical Coherence Tomography Angiography. Ophthalmic Surg Lasers Imaging Retina 2017;48:(8):623–631. [PubMed: 28810037]
25. Uji A, Balasubramanian S, Lei J, Baghdasaryan E, Al-Sheikh M, Sadda SR. Choriocapillaris imaging using multiple en face optical coherence tomography angiography image averaging. JAMA Ophthalmol 2017;135:(11):1197–1204. [PubMed: 28983552]
26. Spaide RF. Choriocapillaris flow features follow a power law distribution: implications for characterization and mechanisms of disease progression. Am J Ophthalmol 2016;170:58–67. [PubMed: 27496785]
27. Chu Z, Chen C-L, Zhang Q, et al. Complex signal-based optical coherence tomography angiography enables in vivo visualization of choriocapillaris in human choroid. J Biomed Opt 2017;22:(12):121705.

28. Choi W, Mohler KJ, Potsaid B, et al. Choriocapillaris and choroidal microvasculature imaging with ultrahigh speed OCT angiography. PLoS ONE 2013;8:(12):e81499. [PubMed: 24349078]
29. Pepple KL, Chu Z, Weinstein J, Munk MR, Van Gelder RN, Wang RK. Use of En Face Swept-Source Optical Coherence Tomography Angiography in Identifying Choroidal Flow Voids in 3 Patients With Birdshot Chorioretinopathy. JAMA Ophthalmol 2018.
30. Otsu N A threshold selection method from gray-level histograms. IEEE Trans Syst Man Cybern 1979;9:(1):62–66.
31. Nesper PL, Soetikno BT, Fawzi AA. Choriocapillaris nonperfusion is associated with poor visual acuity in eyes with reticular pseudodrusen. Am J Ophthalmol 2017;174:42–55. [PubMed: 27794427]
32. Borrelli E, Mastropasqua R, Senatore A, et al. Impact of Choriocapillaris Flow on Multifocal Electroretinography in Intermediate Age-Related Macular Degeneration Eyes. Invest Ophthalmol Vis Sci 2018;59:(4):AMD25–AMD30. [PubMed: 29860309]
33. Alten F, Heiduschka P, Clemens CR, Eter N. Exploring choriocapillaris under reticular pseudodrusen using OCT-Angiography. Graefes Arch Clin Exp Ophthalmol 2016;254:(11):2165–2173. [PubMed: 27193430]
34. Carnevali A, Sacconi R, Corbelli E, et al. Optical coherence tomography angiography analysis of retinal vascular plexuses and choriocapillaris in patients with type 1 diabetes without diabetic retinopathy. Acta diabetol 2017;54:(7):695–702. [PubMed: 28474119]
35. Sugano Y, Sekiryu T, Furuta M, et al. Morphometrical evaluation of the choriocapillaris imaged by swept-source optical coherence tomography angiography. Clin Ophthalmol 2018;12:2267. [PubMed: 30464388]
36. Phansalkar N, More S, Sabale A, Joshi M. Adaptive local thresholding for detection of nuclei in diversity stained cytology images. Communications and Signal Processing (ICCSP), 2011 IEEE International Conference on. 2011:218–220.
37. Borrelli E, Souied EH, Freund KB, et al. Reduced choriocapillaris flow in eyes with type 3 neovascularization and age-related macular degeneration. Retina 2018;38:(10):1968–1976. [PubMed: 29746411]
38. Borrelli E, Shi Y, Uji A, et al. Topographic Analysis of the Choriocapillaris in Intermediate Age-related Macular Degeneration. Am J Ophthalmol 2018;196:34–43. [PubMed: 30118688]
39. Nassisi M, Shi Y, Fan W, et al. Choriocapillaris impairment around the atrophic lesions in patients with geographic atrophy: a swept-source optical coherence tomography angiography study. Br J Ophthalmol 2019;103(7):911–917. [PubMed: 30131381]
40. Nassisi M, Baghdasaryan E, Tepelus T, Asanad S, Borrelli E, Sadda SR. Topographic distribution of choriocapillaris flow deficits in healthy eyes. PloS One 2018;13:(11):e0207638. [PubMed: 30440050]
41. Spaide RF. Choriocapillaris signal voids in maternally inherited diabetes and deafness and in pseudoxanthoma elasticum. Retina 2017;37:(11):2008–2014. [PubMed: 28092344]
42. Rochepeau C, Kodjikian L, Garcia M-A, et al. Optical Coherence Tomography Angiography Quantitative Assessment of Choriocapillaris Blood Flow in Central Serous Chorioretinopathy. Am J Ophthalmol 2018;194:26–34. [PubMed: 30053475]
43. Spaide RF. Ising model of choriocapillaris flow. Retina 2018;38:(1):79–83. [PubMed: 28169877]
44. Meditec CZ. Carl Zeiss Meditec Plex Elite 9000 OCT 501(k) premarket report of FDA, 2016.
45. Yin X, Chao JR, Wang RK. User-guided segmentation for volumetric retinal optical coherence tomography images. J Biomed Opt 2014;19:(8):086020–086020. [PubMed: 25147962]
46. Zhang A, Zhang Q, Wang RK. Minimizing projection artifacts for accurate presentation of choroidal neovascularization in OCT micro-angiography. Biomed Opt Express 2015;6:(10):4130–4143. [PubMed: 26504660]
47. Zhang Q, Zhang A, Lee CS, et al. Projection artifact removal improves visualization and quantitation of macular neovascularization imaged by optical coherence tomography angiography. Ophthalmol Retina 2017;1:(2):124–136. [PubMed: 28584883]
48. Koo TK, Li MY. A guideline of selecting and reporting intraclass correlation coefficients for reliability research. J Chiropr Med 2016;15:(2):155–163. [PubMed: 27330520]

49. Gorczynska I, Migacz J, Jonnal R, Zawadzki R, Poddar R, Werner J. Imaging of the human choroid with a 1.7 MHz A-scan rate FDML swept source OCT system. Ophthalmic Technologies XXVII: International Society for Optics and Photonics, 2017:1004510.

50. Chu Z, Zhang Q, Zhou H, et al. Quantifying choriocapillaris flow deficits using global and localized thresholding methods: a correlation study. Quant Imaging Med Surg, 2018:8(11):1102–1112. [PubMed: 30701164]

51. Xu J, Song S, Men S, Wang RK. Long ranging swept-source optical coherence tomography-based angiography outperforms its spectral-domain counterpart in imaging human skin microcirculations. J Biomed Opt 2017;22:(11):116007.

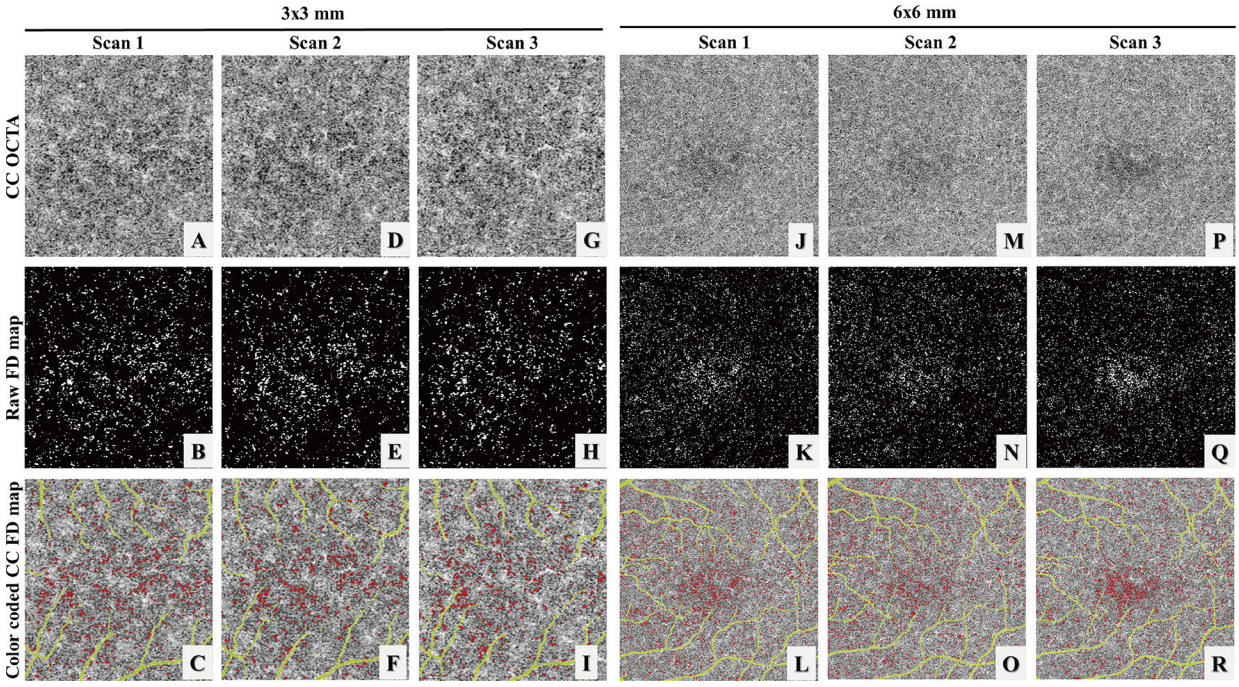

FIGURE 1.

Illustration of the choriocapillaris (CC) using three repeated 3×3 mm scans and 6×6 mm scans from a subject with normal eyes. (**A, D, G, J, M, P**) Swept source optical coherence tomography angiography (SS-OCTA) CC en face images. (**B, E, H, K, N, Q**) binary images of segmented CC flow deficits (FDs) (white) using the fuzzy C-means (FCM) method. (**C, F, I, L, O, R**) color coded CC FD SS-OCTA map (red) after removing FDs below normal inter-capillary distances and projection artifacts (yellow).

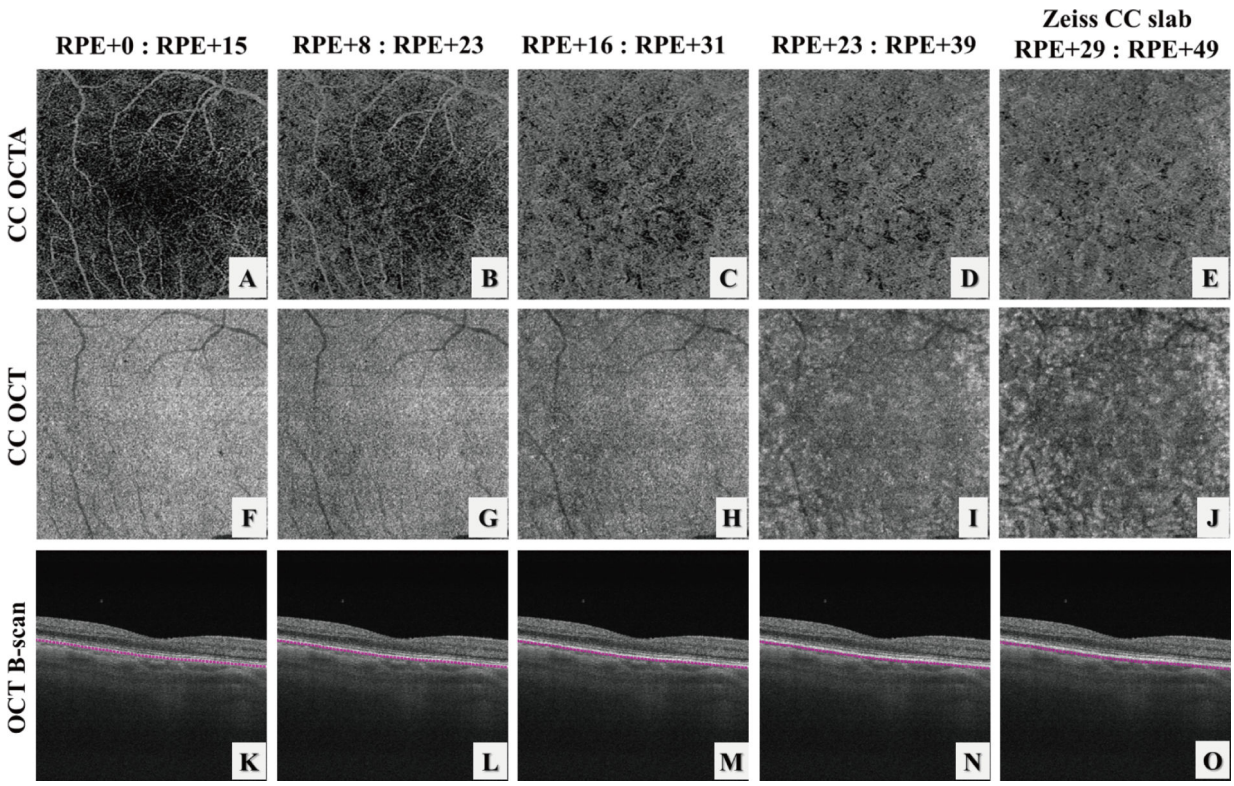

FIGURE 2.

Illustration of the choriocapillaris (CC) appearances with different selections of the CC slab position relative to the RPE in a normal eye using automatic segmentation from the instrument. (**A**-**E**) OCT angiography CC slabs with the selection of positions as shown relative to the RPE position. (**F**-**J**) corresponding OCT CC structural slabs. Note that since the axial pixel size in PLEX® Elite is 1.9 μm/pixel, the slab thickness in (D) and I is 16 μm rather than 15 μm due to rounding issues.

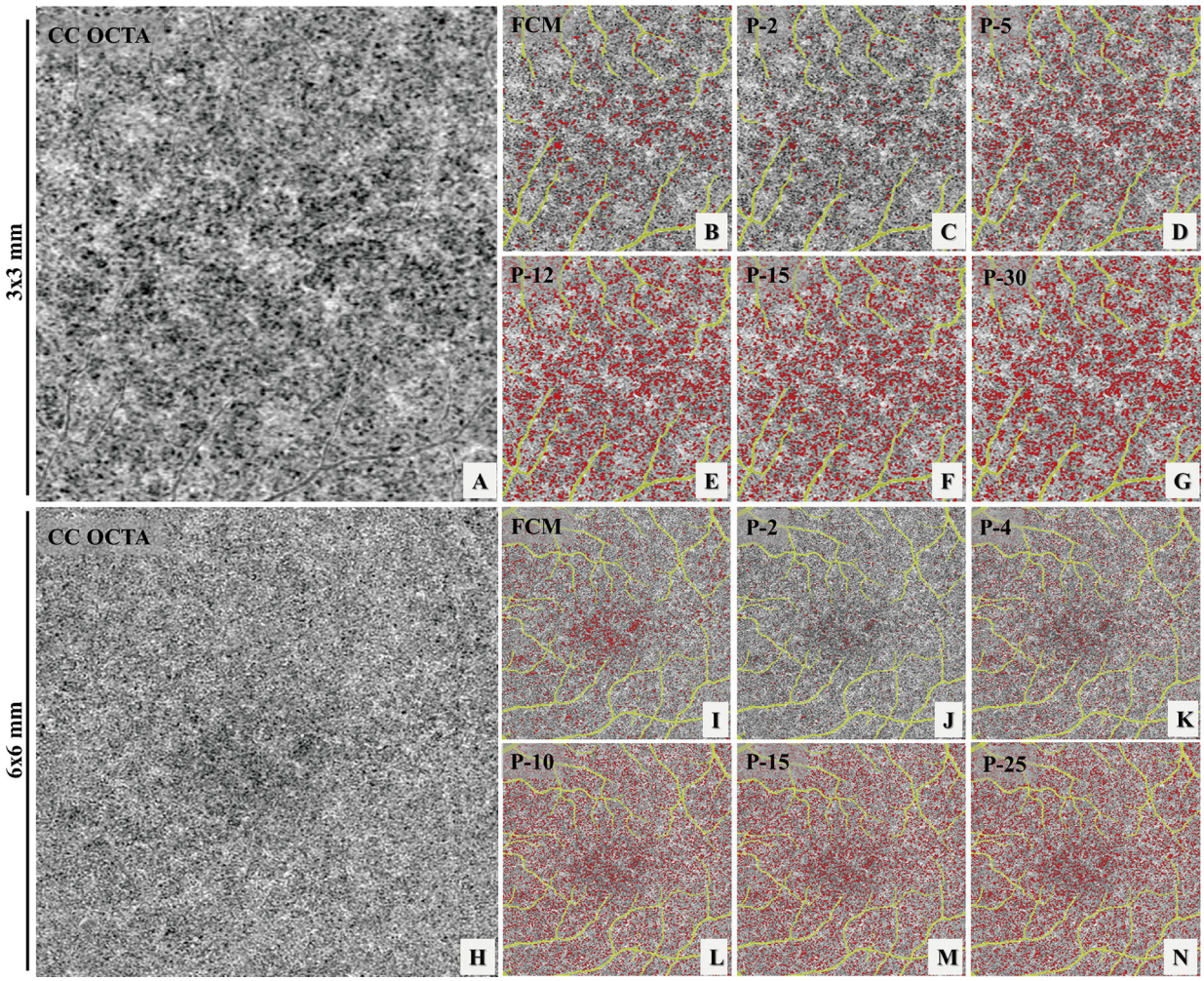

FIGURE 3.

Example of choriocapillaris (CC) flow deficit (FD) segmentation in a subject with normal eyes using both a 3×3 mm averaged scan (A-G) and a 6×6 mm averaged scan (H-N). (**A**) 3×3 mm OCT angiographic (OCTA) CC en face image. (**B**) color coded FD segmentation map (red) using the fuzzy C-means (FCM) method overlaid with the OCTA CC image (grey) and the larger retinal blood vessels (yellow). (**C-G**) color coded FD segmentation map (red) using the Phansalkar method overlaid with OCTA CC image (grey) and the larger retinal vessels (yellow), with 2-pixel radius, 5-pixel radius, 12-pixel radius, 15-pixel radius, and 30-pixel radius, respectively. (**H**) 6×6 mm OCTA CC en face image. (**I**) color coded FD segmentation map (red) by the FCM method overlaid with the OCTA CC en face image (grey) and larger retinal blood vessels (yellow). (**J-N**) color coded FD segmentation map (red) by the Phansalkar method overlaid with the OCTA CC en face image (grey) and larger retinal vessels (yellow), with 2-pixel radius, 5-pixel radius, 12-pixel radius, 15-pixel radius, and 30-pixel radius, respectively.

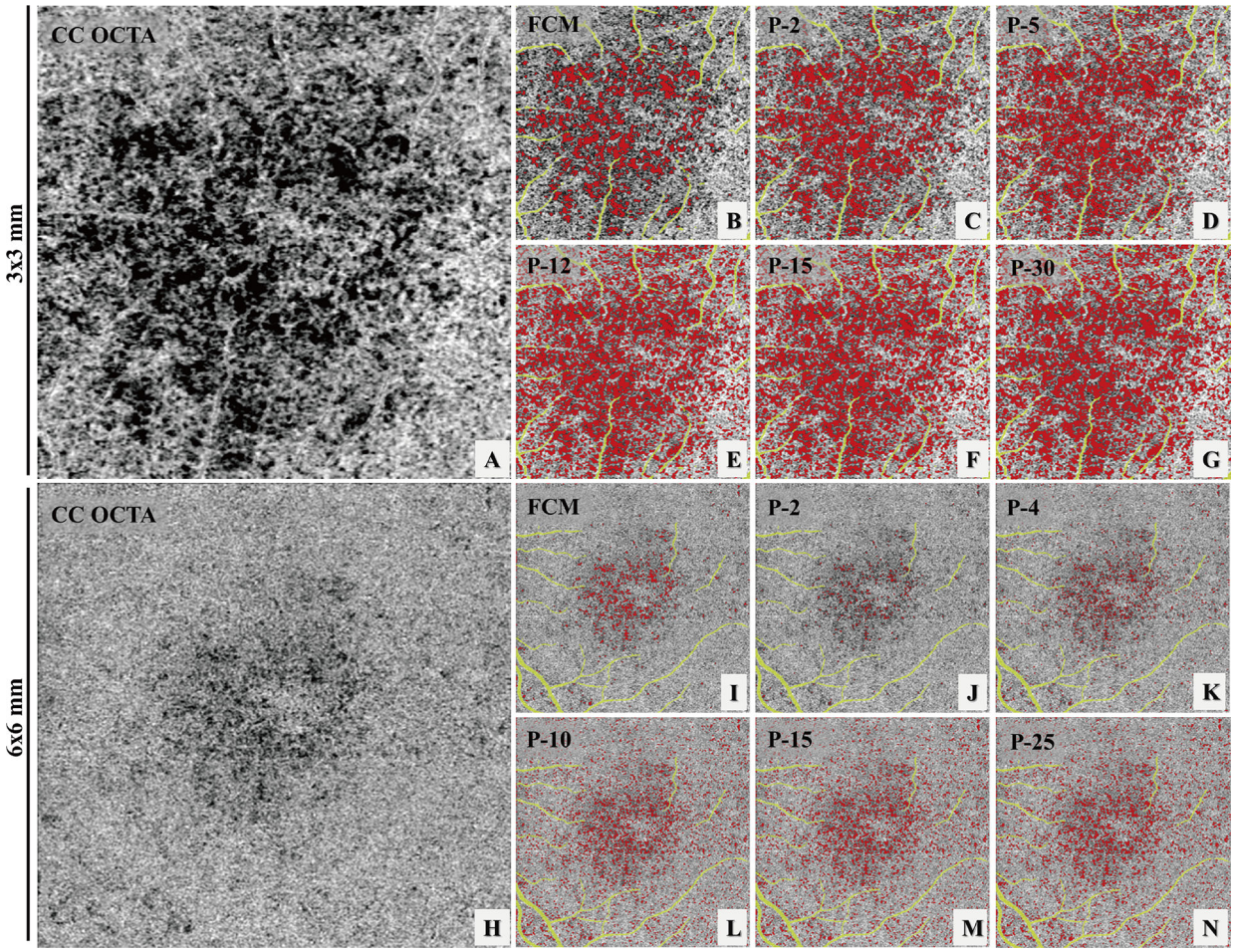

FIGURE 4.

Example of choriocapillaris (CC) flow deficit (FD) segmentation in a 3×3 mm scan (A-G) and a 6×6 mm scan (H-N) acquired from an AMD subject with drusen. (**A**) 3×3 mm OCT angiographic (OCTA) CC en face image. (**B**) color coded FD segmentation map (red) using the fuzzy C-means (FCM) method overlaid with the OCTA CC image (grey) and the larger retinal blood vessels (yellow). (**C-G**) color coded FD segmentation map (red) using the Phansalkar method overlaid with OCTA CC image (grey) and the larger retinal vessels (yellow), with 2-pixel radius, 5-pixel radius, 12-pixel radius, 15-pixel radius, and 30-pixel radius, respectively. (**H**) 6×6 mm OCTA CC en face image. (**I**) color coded FD segmentation map (red) by the FCM method overlaid with the OCTA CC en face image (grey) and larger retinal blood vessels (yellow). (**J-N**) color coded FD segmentation map (red) by the Phansalkar method overlaid with the OCTA CC en face image (grey) and larger retinal vessels (yellow), with 2-pixel radius, 5-pixel radius, 12-pixel radius, 15-pixel radius, and 30-pixel radius, respectively.

TABLE 1.

Intra-class correlation for quantitative metrics used to describe flow deficits (FDs) calculated from the fuzzy C-means (FCM) method and the Phansalkar method using various radius options in 3×3 mm scans of eyes with drusen.

Normal	The FCM method	The Phansalkar method				
		2-pixel radius	4-pixel radius	10-pixel radius	15-pixel radius	30-pixel radius
FDD	0.9598	0.9707	0.9798	0.9792	0.9801	0.9777
MFDS	0.9915	0.9911	0.9795	0.9773	0.9762	0.9804
FDN	0.9687	0.9693	0.9783	0.9318	0.9219	0.8745
ICD	0.9537	0.9967	0.9758	0.9683	0.9653	0.9713
FDA	0.9179	0.9681	0.9775	0.9773	0.9785	0.9771

Abbreviations: FCM, Fuzzy C-means; FD, Flow deficit; FDD, FD density; FDN, FD number; MFDS, mean FD size; ICD, inter-capillary distance; FDA, total FD area.

TABLE 2.

Intra-class correlation for quantitative metrics used to describe flow deficits (FDs) calculated from the fuzzy C-means (FCM) method and the Phansalkar method using various radius options in 3×3 mm scans of eyes with drusen.

Drusen	The FCM method	The Phansalkar method				
		2-pixel radius	4-pixel radius	10-pixel radius	15-pixel radius	30-pixel radius
FDD	0.9492	0.9365	0.9285	0.9201	0.9217	0.9033
MFDS	0.9302	0.9488	0.9215	0.9209	0.8831	0.6625
FDN	0.8762	0.7515	0.8549	0.9377	0.8629	0.9923
ICD	0.8272	0.9368	0.9258	0.8951	0.8712	0.6125
FDA	0.9250	0.9271	0.9183	0.9150	0.9174	0.9803

Abbreviations: FCM, Fuzzy C-means; FD, Flow deficit; FDD, FD density; FDN, FD number; MFDS, mean FD size; ICD, inter-capillary distance; FDA, total FD area.

TABLE 3.

Intra-class correlation for quantitative metrics used to describe flow deficits (FDs) calculated from the fuzzy C-means (FCM) method and the Phansalkar method using various radius options in 6×6 mm scans of eyes with drusen.

Normal	The FCM method	The Phansalkar method				
		2-pixel radius	4-pixel radius	10-pixel radius	15-pixel radius	25-pixel radius
FDD	0.9287	0.7732	0.9507	0.9478	0.9526	0.9637
MFDS	0.9140	0.8760	0.9301	0.9668	0.9733	0.9786
FDN	0.9544	0.9498	0.9526	0.9293	0.9336	0.9436
ICD	0.9435	0.9072	0.9600	0.9643	0.9663	0.9789
FDA	0.9598	0.9418	0.9546	0.9539	0.9585	0.9688

Abbreviations: FCM, Fuzzy C-means; FD, Flow deficit; FDD, FD density; FDN, FD number; MFDS, mean FD size; ICD, inter-capillary distance; FDA, total FD area.

TABLE 4.

Intra-class correlation for quantitative metrics used to describe flow deficits (FDs) calculated from the fuzzy C-means (FCM) method and the Phansalkar method using various radius options in 6×6 mm scans of eyes with drusen.

Drusen	The FCM method	The Phansalkar method				
		2-pixel radius	4-pixel radius	10-pixel radius	15-pixel radius	25-pixel radius
FDD	0.8045	0.5697	0.6647	0.7630	0.7848	0.7448
MFDS	0.9152	0.7943	0.7153	0.6910	0.7517	0.7319
FDN	0.8786	0.5684	0.7076	0.7819	0.7740	0.7165
ICD	0.9115	0.7000	0.6872	0.6727	0.7658	0.7382
FDA	0.8703	0.5605	0.6415	0.7399	0.7652	0.7171

Abbreviations: FCM, Fuzzy C-means; FD, Flow deficit; FDD, FD density; FDN, FD number; MFDS, mean FD size; ICD, inter-capillary distance; FDA, total FD area.

TABLE 5.

Descriptive statistics for several choriocapillaris (CC) metrics in the 3×3 mm scans over a l 12 subjects.

Mean (SD)	The FCM method	The Phansalkar method					ANOVA test
		2-pixel radius	5-pixel radius	12-pixel radius	15-pixel radius	25-pixel radius	
FDD, % (SD)	7.62 (3.60)	13.66 (8.18)	22.03 (7.57)	27.85 (6.68)	28.51 (6.58)	29.6 (6.27)	p<0.001
MFDS, μm (SD)	1703.6 (766.9)	1679.4 (881.0)	1718.8 (733.0)	2597.8 (1033.5)	2885.6 (1155.6)	3475.2 (1389.7)	p<0.001
FDN (SD)	361.9 (24.1)	632.6 (150.4)	1082.5 (156.1)	931.8 (166.5)	862.6 (161.1)	748.0 (149.8)	p<0.001
ICD, μm (SD)	33.0 (5.0)	33.0 (5.5)	33.2 (4.7)	40.9 (5.5)	42.8 (5.6)	45.5 (5.5)	p<0.001
FDA, μm2 (SD)	0.79 (0.25)	1.11 (0.64)	1.80 (0.60)	2.27 (0.54)	2.33 (0.53)	2.42 (0.51)	p<0.001

Abbreviations: FCM, Fuzzy C-means; SD, standard deviation; FD, Flow deficit; FDD, FD density; FDN, FD number; MFDS, mean FD size; ICD, inter-capillary distance; FDA, total FD area.

TABLE 6.

Descriptive statistics for several choriocapillaris (CC) metrics in the 6×6 mm scans over a l 12 subjects.

Mean (SD)	The FCM method	The Phansalkar method					ANOVA test
		2-pixel radius	5-pixel radius	12-pixel radius	15-pixel radius	30-pixel radius	
FDD, % (SD)	3.98 (0.93)	1.75 (0.48)	6.20 (1.37)	14.04 (2.13)	15.09 (2.17)	15.65 (2.30)	p<0.001
MFDS, μm (SD)	1233.0 (324.5)	847.8 (151.8)	864.1 (84.1)	1292.3 (96.1)	1475.6 (135.6)	1619.8 (175.0)	p<0.001
FDN (SD)	1160.4 (457.6)	687.4 (174.0)	2392.2 (621.5)	3577.4 (566.9)	3373.1 (520.0)	3191.8 (515.7)	p<0.001
ICD, μm (SD)	28.7 (2.3)	24.7 (1.9)	25.0 (1.0)	30.9 (1.0)	32.9 (1.2)	34.3 (1.3)	p<0.001
FDA, μm2 (SD)	1.80 (0.49)	0.58 (0.17)	2.04 (0.46)	4.61 (0.71)	4.96 (0.72)	5.14 (0.77)	p<0.001

Abbreviations: FCM, Fuzzy C-means; SD, standard deviation; FD, Flow deficit; FDD, FD density; FDN, FD number; MFDS, mean FD size; ICD, inter-capillary distance; FDA, total FD area.

TABLE 7.

Pearson's correlations between the fuzzy C-means (FCM) method and the Phansalkar method in the 3×3 mm scans.

3×3	The FCM method& the Phansalkar method (2-pixel radius)	The FCM method& the Phansalkar method (5-pixel radius)	The FCM method& the Phansalkar method (12-pixel radius)	The FCM method& the Phansalkar method (15-pixel radius)	The FCM method& the Phansalkar method (30-pixel radius)
FDD	r = 0.98, p < 0.001	r = 0.96, p < 0.001	r = 0.94, p < 0.001	r = 0.94, p < 0.001	r = 0.94, p < 0.001
MFDS	r = 0.99, p < 0.001	r = 0.99, p < 0.001	r = 0.97, p < 0.001	r = 0.97, p < 0.001	r = 0.96, p < 0.001
FDN	r = 0.26, p = 0.46	r = 0.05, p = 0.88	r = −0.14, p = 0.69	r = −0.16, p = 0.65	r = −0.20, p = 0.58
ICD	r = 0.99, p < 0.001	r = 0.96, p < 0.001	r = 0.92, p < 0.001	r = 0.90, p < 0.001	r = 0.87, p < 0.001
FDA	r = 0.97, p < 0.001	r = 0.94, p < 0.001	r = 0.90, p < 0.001	r = 0.90, p < 0.001	r = 0.89, p < 0.001

Abbreviations: FCM, Fuzzy C-means; SD, standard deviation; FD, Flow deficit; FDD, FD density; FDN, FD number; MFDS, mean FD size; ICD, inter-capillary distance; FDA, total FD area.

TABLE 8.

Pearson's correlations between the fuzzy C-means (FCM) method and the Phansalkar method in the 6×6 mm scans.

6×6	The FCM method& the Phansalkar method (2-pixel radius)	The FCM method& the Phansalkar method (4-pixel radius)	The FCM method& the Phansalkar method (10-pixel radius)	The FCM method& the Phansalkar method (15-pixel radius)	The FCM method& the Phansalkar method (25-pixel radius)
FDD	r = −0.04, p = 0.93	r = 0.68, p = 0.03	r = 0.71, p = 0.02	r = 0.69, p = 0.03	r = 0.68, p = 0.03
MFDS	r = 0.96, p < 0.001	r= 0.91, p < 0.001	r = 0.45, p = 0.19	r = 0.45, p = 0.19	r = 0.51, p = 0.13
FDN	r = 0.49, p = 0.15	r = 0.85, p = 0.002	r = 0.91, p < 0.001	r = 0.94, p < 0.001	r = 0.95, p < 0.001
ICD	r = 0.93, p < 0.001	r = 0.93, p < 0.001	r = 0.52, p = 0.13	r = 0.46, p = 0.18	r = 0.63, p = 0.06
FDA	r = −0.04, p = 0.93	r = 0.68, p = 0.03	r = 0.70, p = 0.02	r = 0.67, p = 0.03	r = 0.66, p = 0.04

Abbreviations: FCM, Fuzzy C-means; SD, standard deviation; FD, Flow deficit; FDD, FD density; FDN, FD number; MFDS, mean FD size; ICD, inter-capillary distance; FDA, total FD area.